Applied Catalysis B: Environmental 236 (2018) 359–367

Contents lists available at ScienceDirect

Applied Catalysis B: Environmental

journal homepage: www.elsevier.com/locate/apcatb

Spontaneous weaving: 3D porous PtCu networks with ultrathin jagged nanowires for highly efficient oxygen reduction reaction

Jie Ying, Gaopeng Jiang, Zachary P. Cano, Zhong Ma, Zhongwei Chen*

Department of Chemical Engineering, University of Waterloo, Ontario, N2L 3G1, Canada

ARTICLE INFO

Keywords:
3D porous materials
Pt-based alloys
Morphological evolution
Nanostructures
Oxygen reduction reaction

ABSTRACT

We report a simple and efficient surfactant-free method to prepare 3D porous PtCu networks with ultrathin jagged nanowires and controllable composition. The morphological evolution and the influential effects of the important experimental parameters on the PtCu networks have been systematically studied. Relative to commercial Pt/C and Pt black catalysts, these porous PtCu networks exhibit much better activity and remarkably improved durability towards the oxygen reduction reaction (ORR). The excellent ORR performance could be attributed to their structural features, including the core-shell nanostructures with a Pt-skin, the 3D porous networks with high surface area, and the ultrathin (3.6 nm) jagged nanowires with plentiful edge/corner atoms. Notably, this method can be facilely extended to obtain PtCuAu trimetallic nanowire networks with high porosity, which exhibits its robustness for preparing novel 3D porous nanostructures with great potential in various catalytic applications.

1. Introduction

Pt-based nanostructures have received considerable attention due to their unique properties in various applications, such as catalysis, electrochemistry, and sensors [1–5]. Among these applications, proton exchange membrane fuel cells (PEMFCs) represent one of the most promising power sources for electric vehicles and portable electronic devices owing to their relatively high energy conversion efficiency, low operation temperature, and non-polluting emissions [2,6]. However, the promise of their wide commercial application is seriously hindered by the high cost, insufficient activity and poor durability of Pt-based catalysts for the sluggish oxygen reduction reaction (ORR) at the cathode [7]. Moreover, since carbon-supported Pt-based catalysts are the most widely-used ORR catalysts, the corrosion of carbon supports during the start-up and shut-down cycling and long-term operational conditions is a serious issue which results in a significant loss of ORR activity and PEMFC performance [8]. Therefore, the development of advanced Pt-based electrocatalysts with reduced Pt mass, enhanced catalytic activity and durability, and corrosion-resistant carbon supports is strongly demanded for the efficiency and commercial viability of PEMFCs.

One of the effective strategies to improve the performance and utilization efficiency of Pt-based catalysts is to prepare porous nanostructures with large surface area and high porosity, such as branched/dendritic nanocrystals [9,10], nanotubes [11,12], nanoframes [13,14], porous films and networks [15–17]. Among them, 3D porous networks are a unique and promising class of nanomaterials, featuring low densities, large open interconnected pores, and abundant active sites [16,18]. These 3D porous networks of weaved nanowire units not only own the inherent features of 1D nanostructured catalysts (i.e., high stability, fast electron transport, and highly-exposed active sites) [19,20], but can also demonstrate improved catalytic performance as one on the macroscale relative to their component units due to their enhanced collective properties [21]. Furthermore, the structural rigidity of 3D porous networks allows them to serve as support-free electrocatalysts to eliminate the carbon corrosion issue in conventional electrocatalysts. Thus, the exploration of novel 3D porous networks as electrocatalysts is of great interest.

Over the past decades, many synthetic approaches have been successfully exploited for preparing noble-metal-based 3D porous networks, such as hard templating, dealloying, and galvanic replacement. However, harsh and/or complex procedures or sacrificial materials were required, rendering these techniques difficult to perform at commercial scale [22,23]. Recently, self-assembly has been developed as a simple and effective method for creating 3D porous networks [16–18,24–26]. For example, Eychmüller et al. reported a facile method for producing 3D porous Pd networks by directly reducing Pd salts using sodium borohydride as the reducing agent in the presence of cyclodextrin [16]. Arachchige et al. reported a salt-mediated self-assembly of metal nanoshells into 3D porous bimetallic networks (AuAg,

* Corresponding author.
E-mail addresses: zhwchen@uwaterloo.ca, d28luo@uwaterloo.ca (Z. Chen).

https://doi.org/10.1016/j.apcatb.2018.04.035
Received 3 January 2018; Received in revised form 13 April 2018; Accepted 17 April 2018
Available online 19 April 2018

PdAg, and PtAg) [24]. Despite the above successful demonstrations, it has to be pointed out that the fabrication of noble-metal-based 3D porous networks is still very limited in comparison with other traditional materials (such as oxides, carbons, non-noble metals). More importantly, two major challenges in the synthesis of noble-metal-based 3D porous networks should be addressed prior to their practical application in PEMFCs. The first is the development of simple, efficient and environmentally-friendly strategies which can be performed at an industrial scale. Reported synthetic procedures have at least one disadvantage in this regard, including multistep, long reaction times (several days to months), high reaction temperatures, and the use of surfactants as structure-directing agents. The second challenge is to allow the introduction of non-noble metals to form bi-/trimetallic alloys. This would lower costs by reducing the use of noble metals, while enabling enhanced activity and stability of noble-metal-based electrocatalysts by exploiting the synergetic effects between each metal [27].

To address these challenges, we report herein a simple and effective approach for the preparation of 3D porous PtCu with ultrathin nanowire networks and controllable composition. The technique, which involves direct reduction of metal precursors in an aqueous solution at room temperature, requires no surfactants and can be performed within hours. The morphological evolution and the influence of the major synthesis parameters on the final products have been systematically investigated. The obtained PtCu porous networks, as support-free ORR electrocatalysts, exhibit a highly superior activity and significantly improved durability in comparison with commercial Pt/C and Pt black catalysts. Furthermore, tri-metallic PtCuAu with 3D porous nanowire networks can be readily synthesized by addition and co-reduction of Au precursor with Pt and Cu, demonstrating the flexibility and feasibility of our method for creating novel 3D porous nanoarchitectures.

2. Experimental section

2.1. Synthesis of porous PtCu networks

In a typical synthesis of porous $Pt_{76}Cu_{24}$ networks, aqueous solutions of H_2PtCl_6 (129 μL, 30 mM) and $CuCl_2$ (43 μL, 30 mM) were mixed in a vial with deionized water (15 mL). Then, freshly prepared $NaBH_4$ (0.35 mL, 50 mM) aqueous solution was added into the vial under sonication for 1 min at room temperature. The resulting mixture was kept in the static state for about 8 h at room temperature. The products were collected by centrifugation and washed two times with deionized water. $Pt_{52}Cu_{48}$ and $Pt_{28}Cu_{72}$ networks were synthesized using the same synthesis procedure with different molar ratios of Pt and Cu precursors (86 μL of 30 mM H_2PtCl_6 and 86 μL of 30 mM of $CuCl_2$ for $Pt_{52}Cu_{48}$, 43 μL of 30 mM H_2PtCl_6 and 129 μL of 30 mM of $CuCl_2$ for $Pt_{28}Cu_{72}$).

2.2. Synthesis of porous PtCuAu networks

In a typical synthesis of porous PtCuAu networks, aqueous solutions of H_2PtCl_6 (43 μL, 30 mM), $CuCl_2$ (86 μL, 30 mM), and $HAuCl_4$ (43 μL, 30 mM) were mixed in a vial with deionized water (15 mL). Then, fresh $NaBH_4$ (0.35 mL, 50 mM) aqueous solution was added into the vial under sonication for 1 min at room temperature. The resulting mixture was kept in the static state for about 8 h at room temperature. The products were collected by centrifugation and washed two times with deionized water.

2.3. Characterization

XRD measurements were conducted on a XRG 3000 diffractometer equipped with Cu Kα radiation. SEM and TEM images were carried out on LEO FESEM 1530 and JEOL2010F microscopes, respectively. The nitrogen adsorption and desorption isotherms were collected on a Micromeritics ASAP 3020 system. The outgas temperature for all adsorption/desorption measurements was 80 °C (maintained overnight). The elemental contents in the catalysts were measured by ICP-AES (Perkin Elmer Ltd., USA). The chemical surface characteristics were measured with XPS (Thermal Scientific K-Alpha).

2.4. Electrochemical measurements

All electrochemical measurements were conducted in a three-electrode cell at room temperature. A platinum wire and reversible hydrogen electrode were used as counter and reference electrodes, respectively. A glassy-carbon rotating disk electrode (RDE, diameter: 5 mm, area: 0.196 cm^2) served as the substrate for the working electrode. The Pt loadings of all PtCu samples on glassy-carbon were 15.0 μg cm^{-2}. CV measurements were performed in N_2-saturated 0.1 M $HClO_4$ solution at a sweep rate of 50 mV s^{-1}. ORR measurements were conducted in O_2-saturated 0.1 M $HClO_4$ solution at a rotation rate of 1600 rpm with a sweep rate of 10 mV s^{-1}. The accelerated durability tests were carried out in O_2-saturated 0.1 M $HClO_4$ solution by applying cyclic potential sweeps between 0.6 and 1.1 V versus RHE at a sweep rate of 50 mV s^{-1} for different cycles. For comparison, commercial Pt/C catalyst (TKK, 28.2 wt% Pt) and Pt black (Sigma-Aldrich, 99.9% fuel cell grade) were used as the baseline catalysts, and the same procedure as described above was used to perform the electrochemical measurements, except that the Pt loadings were 20.0 μg cm^{-2} and 51.0 μg cm^{-2} for commercial Pt/C and Pt black catalysts, respectively.

3. Results and discussion

The morphology and structure of as-synthesized $Pt_{76}Cu_{24}$ were initially investigated by electron microscopy. As shown in Fig. 1a, the representative scanning electron microscopy (SEM) image shows that $Pt_{76}Cu_{24}$ displays a typical three-dimensional porous nanostructure with open interconnected pores and ultrathin nanowire networks. These porous networks, constructed by ultrathin and jagged nanowires with an average diameter of 3.6 nm, are clearly presented in the high-angle annular dark-field scanning transmission electron microscopy (HAADF-STEM) and TEM images (Fig. 1b,c). Selected-area electron diffraction (SAED) of $Pt_{76}Cu_{24}$ reveals a polycrystalline diffraction pattern of concentric rings, which can be assigned to (111), (200), (311), and (222) planes of face-centered cubic (fcc) PtCu (Inset of Fig. 1c), indicating the highly crystalline degree of these porous networks. To identify the crystalline structure of the individual nanowires, some common locations in $Pt_{76}Cu_{24}$ networks including one branch-free end, one cross-linked area, and one curved loop are characterized by high-resolution TEM (HRTEM) and the fast Fourier transformation (FFT) (Fig. 1d–f). All of these images reveal that $Pt_{76}Cu_{24}$ networks show clear atomic lattices with variable orientation. Notably, these nanowires exhibit jagged nanostructures with plentiful atomic edges and corners, which would be advantageous for their catalytic applications.[19,27] The widely distributed fringes with lattice spacings of 0.22 nm, 0.19 nm and 0.14 nm can be assigned respectively to the (111), (200) and (220) planes of fcc PtCu. To investigate the elemental distribution, elemental maps of an individual nanowire in $Pt_{76}Cu_{24}$ networks were collected with HAADF-STEM energy-dispersive X-ray spectroscopy (HAADF-STEM-EDX). As shown in Fig. 1 g, Pt elements are distributed throughout the whole nanowire while Cu elements are only located in the center along the nanowire, showing a typical core-shell nanostructure. This $Pt_{76}Cu_{24}$ bimetallic core-shell structure is further confirmed by HAADF-STEM-EDX line scanning analyses (Fig. 1h).

X-ray photoelectron spectroscopy (XPS) spectra of characteristic Pt

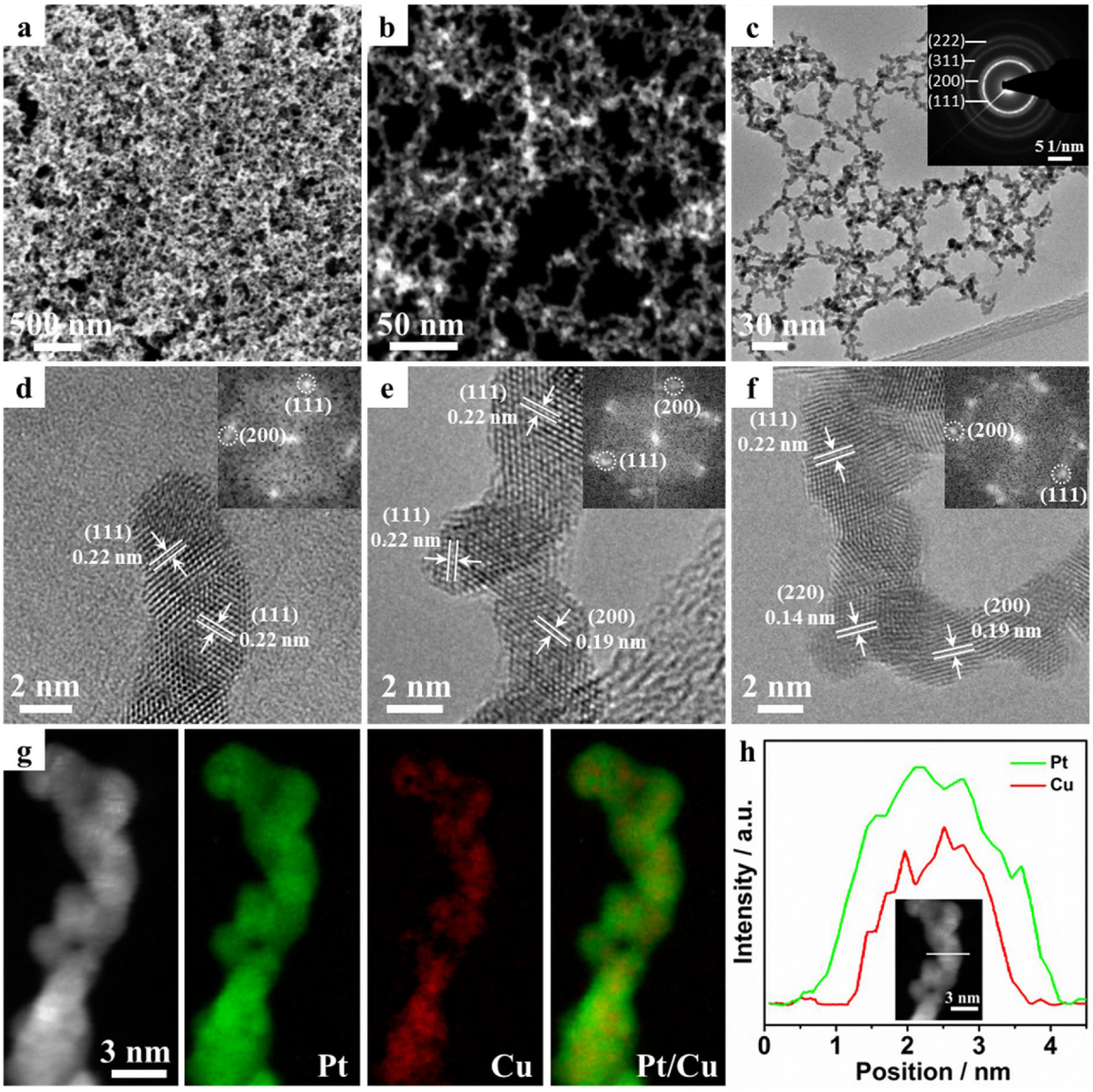

Fig. 1. (a) SEM, (b) HAADF-STEM, and (c) TEM images of as-synthesized $Pt_{76}Cu_{24}$ networks. Inset in c) is the SAED pattern recorded from c). HRTEM images of as-synthesized $Pt_{76}Cu_{24}$ networks with (d) one branch-free end, (e) one cross-linked area, and (f) one curved loop. The insets in d–f) are their corresponding FFT patterns. (g) HAADF-STEM image and EDX mapping images of an individual nanowire in as-synthesized $Pt_{76}Cu_{24}$ networks. (h) HAADF-STEM image and EDX line profiles of a branch in an individual nanowire in as-synthesized $Pt_{76}Cu_{24}$ networks.

and Cu peaks for $Pt_{76}Cu_{24}$ networks are shown in Fig. S1. Analysis of the Pt 4f and Cu 2p spectra indicates that ~ 90% surface Pt and ~ 100% surface Cu are in the metallic state while ~ 10% surface Pt are in the oxidized state. Meanwhile, as measured by inductively coupled plasma atomic emission spectroscopy (ICP-AES) (Table S1), the overall Pt and Cu molar ratio in $Pt_{76}Cu_{24}$ is about 3:1, which is consistent with the supplied Pt/Cu atomic ratio in the initial reaction, indicating that the Pt and Cu precursors are fully utilized during the synthesis. The crystallinity of $Pt_{76}Cu_{24}$ networks was also investigated by powder X-ray diffraction (XRD) (Fig. S2). The three distinct peaks correspond to (111), (200), and (220) planes of the fcc PtCu crystal structure, which is in good agreement with the SAED results. Compared to the corresponding peaks of Pt (JCPDS no. 04–0802), the peaks in $Pt_{76}Cu_{24}$ networks show an obvious shift to higher 2 theta due to the influence of Cu in forming PtCu bimetallic nanostructures by contraction of the lattice parameters [28]. The highly porous nature of $Pt_{76}Cu_{24}$ networks was further confirmed by nitrogen adsorption-desorption measurement (Fig. S3a). The surface area of $Pt_{76}Cu_{24}$ networks determined by the Brunauer-Emmett-Teller (BET) method shows a very high value of 126 $m^2\ g^{-1}$, which is much higher than the reported Pt-based porous nanomaterials [17,29–31]. Such a high surface area comes from the 3D porous interconnected nanostructure consisting of ultrathin and jagged nanowires.

To reveal the structural evolution of $Pt_{76}Cu_{24}$ networks during self-assembly, the intermediate nanostructures synthesized at different reaction durations are investigated by TEM. In the initial stage of the reaction (10 s), small nanoparticles are observed, with some of them beginning to coalesce (Fig. 2a). After 1 min, well-defined nanowires with jagged nanostructures are formed and linked with each other (Fig. 2b). With prolonged reaction time (5, 10 and 15 min), the jagged

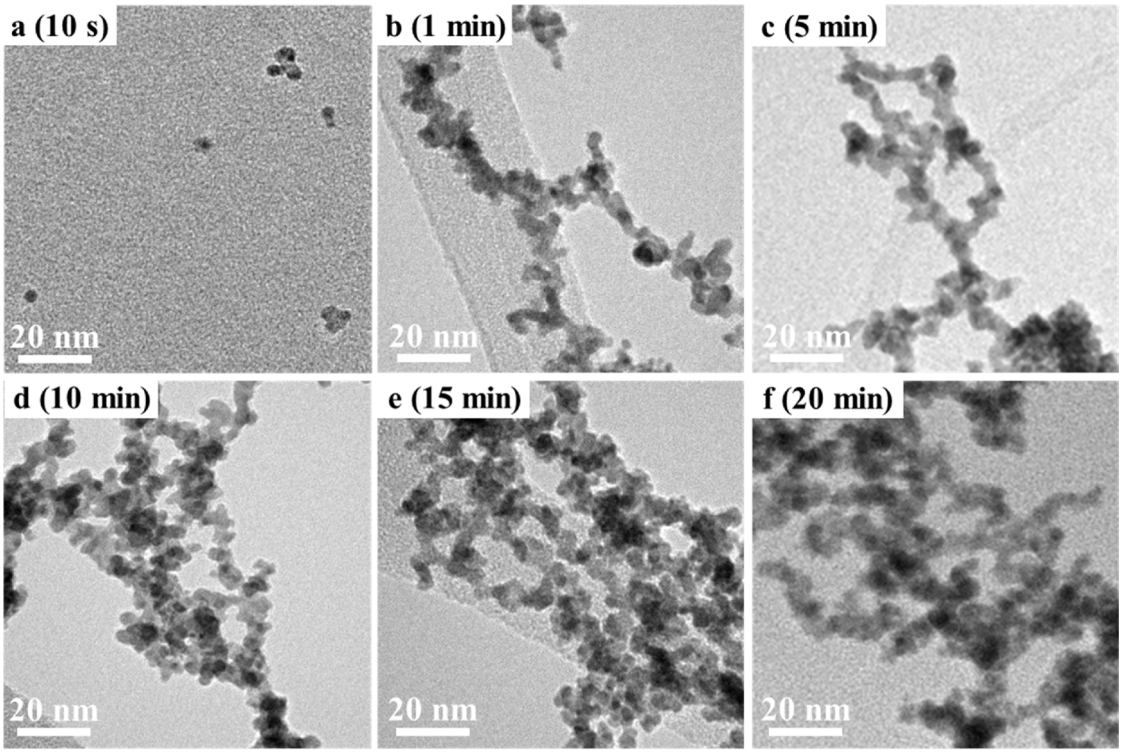

Fig. 2. TEM images of the products obtained at different reaction durations: (a) 10 s; (b) 1 min; (c) 5 min; (d) 10 min; (e) 15 min; and (f) 20 min.

nanowires begin to evolve to porous networks with increasing interconnectedness (Fig. 2c-e). The growth step is found to be completed after 20 min since there is no obvious change after prolonged reaction time (Fig. 2f). As shown in Fig. S4, the growth solution changed from transparent to black within 20 min after adding the reducing agent. These black products were completely settled at the bottom of the vial after 8 h, and upon removal they were observed to be interlocked. Thus, during settlement after 20 min, these nanowire networks are further interweaved to form 3D porous networks on the macroscale (as shown in Fig. 1a). These results suggest that the morphological evolution of $Pt_{76}Cu_{24}$ in our case is a spontaneous weaving process including the progression from small nanoparticles to jagged nanowires, nanowire knots, nanowire networks, and finally to macroscopic porous networks.

Additional control experiments were also conducted to further understand the growth mechanism of $Pt_{76}Cu_{24}$ networks. In our synthesis, the choice of using $NaBH_4$ as the reduction agent is critical for the formation of $Pt_{76}Cu_{24}$ nanowire networks. When $NaBH_4$ was replaced by hydrazine (N_2H_4, another commonly used strong reducing agent), large irregular nanoparticle aggregates formed instead of nanowire networks (Fig. S5). Additionally, controlling the reaction at room temperature was not necessary for the formation of nanostructured networks, but was important to obtain $Pt_{76}Cu_{24}$ networks with high quality and high dispersion. When the reaction temperature increased from room temperature to 50 °C, the obtained nanowire networks were partly aggregated, leading to low quality of porous nanostructures (Fig. S6a,b). This could be attributed to the faster growth kinetics during the synthesis. With increasing the reaction temperature to 80 °C, severe aggregation of the nanowire networks occurred (Fig. S6c,d). In addition, when only H_2PtCl_6 was used as a metal precursor, nanowire networks with only slightly increased average diameter of 7.8 nm and multangular surfaces were presented (Fig. 3a,b). However, when only $CuCl_2$ was used, nanowire networks with even larger diameter (over 10.0 nm), smooth surfaces, and low dispersity were formed (Fig. 3c,d). This result indicates that the interaction between Pt and Cu precursors during the synthesis is integral to the formation of well-defined $Pt_{76}Cu_{24}$ networks with ultrathin nanowires. Moreover, the composition of $Pt_{76}Cu_{24}$ bimetallic nanowire networks can be readily controlled by simply adjusting the ratios of the Pt and Cu precursors. Based on ICP-AES measurements, when the molar ratios of Pt/Cu precursors were changed to 1:1 and 1:3, the Pt/Cu molar ratio in the obtained products are close to 1:1 and 1:3 (denoted as $Pt_{52}Cu_{48}$ and $Pt_{28}Cu_{72}$), respectively (Table S1). The TEM images of $Pt_{52}Cu_{48}$ and $Pt_{28}Cu_{72}$ reveal their well-defined nanowire networks to be similar in appearance to $Pt_{76}Cu_{24}$ (Fig. 3e-h). The XRD analyses (Fig. S2a) confirmed the high crystallinity of $Pt_{52}Cu_{28}$ and $Pt_{28}Cu_{72}$. Meanwhile, with increasing Pt content, the peaks for the PtCu (111) plane exhibit a clear shift to lower 2 theta values (Fig. S2b), which is consistent with a previous report [32]. The nitrogen adsorption-desorption measurements (Fig. S3b,c) demonstrate the high porosity of $Pt_{52}Cu_{28}$ and $Pt_{28}Cu_{72}$, with high surface areas of 118 $m^2\ g^{-1}$ and 109 $m^2\ g^{-1}$, respectively.

In contrast to the previously reported noble-metal-based porous nanostructures, the synthesis of $Pt_{76}Cu_{24}$ networks described here has remarkable advantages in the following aspects. First, this method is a highly convenient and efficient synthesis strategy without the need for surfactants, organic solvents, as-synthesized seeds, hard templates, high reaction temperatures, or long reaction times, all of which are highly desirable for scaling up in commercial applications. Second, the high porosity and surface area of the 3D porous networks could greatly promote mass transport and surface exposure for catalytic processes. Third, the highly interconnected and interwoven structure could provide a strong self-supporting capability while minimizing interfacial electronic resistance, thus allowing for avoidance of corrosion-prone carbon supports. Finally, the ultrathin and jagged nanowire subunits with abundant edge/corner atoms can further maximize the catalytic

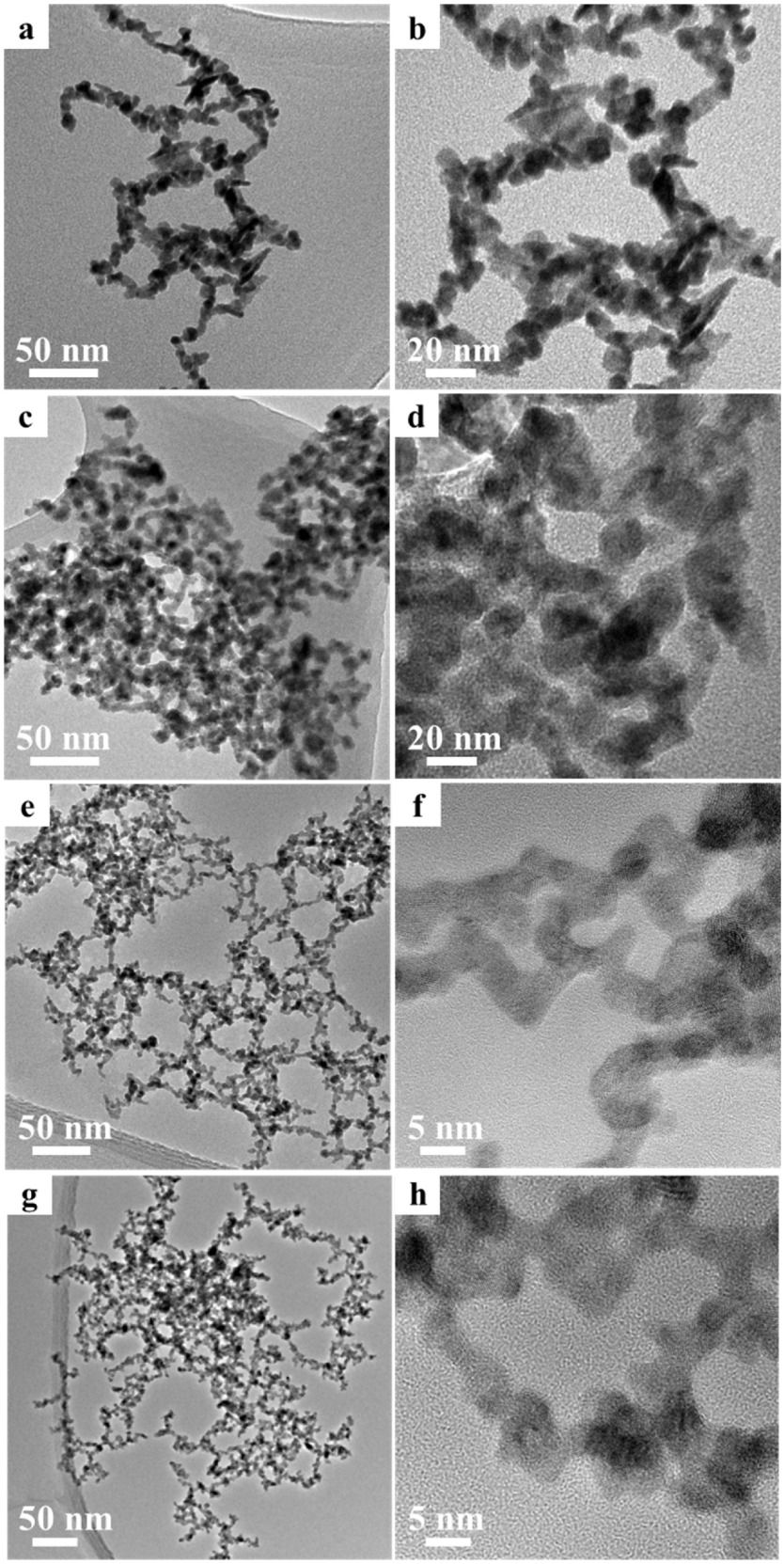

Fig. 3. TEM images of the products from the reaction with the same conditions used in the synthesis of $Pt_{76}Cu_{24}$, but with solely (a,b) Pt precursor (H_2PtCl_6) and (c,d) Cu precursor ($CuCl_2$). TEM images of the products from the reaction with the same conditions used in the synthesis of $Pt_{76}Cu_{24}$, but using different Pt/Cu molar ratios: (e,f) 1:1; and (g,h) 1:3.

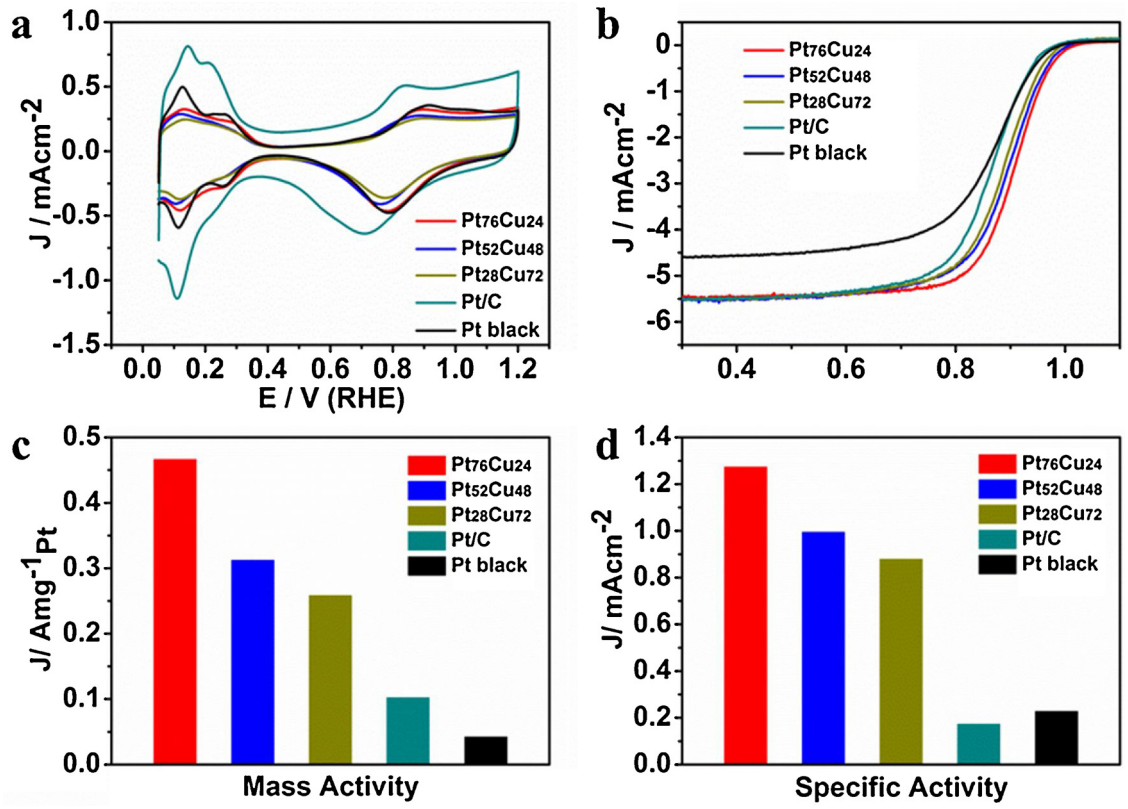

Fig. 4. (a) CV curves recorded at room temperature in N_2-satured 0.1 M $HClO_4$ solution with a sweep rate of 50 mV s^{-1}, (b) ORR polarization curves recorded at room temperature in O_2-satured 0.1 M $HClO_4$ solution with a sweep rate of 10 mV s^{-1} and a rotation rate of 1600 rpm, (c) mass activity, and (d) specific activity at 0.9 V versus RHE for $Pt_{76}Cu_{24}$, $Pt_{52}Cu_{48}$, $Pt_{28}Cu_{72}$, Pt/C, and Pt black catalysts.

activity and utilization efficiency of the metal catalysts while exploiting the intrinsic high stability of 1D nanowires. Thus, the as-prepared $Pt_{76}Cu_{24}$ networks are very attractive candidates for electrocatalysis, and can be expected to display superior catalytic performance and stability to incumbent catalysts for PEMFCs.

The electrocatalytic properties of all the PtCu networks ($Pt_{76}Cu_{24}$, $Pt_{52}Cu_{48}$ and $Pt_{28}Cu_{72}$) toward the ORR were investigated. Commercial Pt/C and Pt black catalysts were also evaluated as references. Fig. 4a shows cyclic voltammetry (CV) curves of all these catalysts recorded in N_2-satured 0.1 M $HClO_4$ solution at room temperature with a sweep rate of 50 mV s^{-1}. The electrochemically active surface area (ECSA) was calculated by measuring the charge collected in the hydrogen adsorption/desorption region after double-layer correction and assuming that the value for the adsorption of a hydrogen monolayer is 0.21 mC cm^{-2}. Based on the Pt mass, the ECSA values for $Pt_{76}Cu_{24}$, $Pt_{52}Cu_{48}$, $Pt_{28}Cu_{72}$, Pt/C, and Pt black catalysts are 36.6, 31.4, 29.4, 58.9 and 18.5 m^2 g^{-1}, respectively (Fig. S7 and Table S2). With respect to the previously reported Pt-based nanostructures constructed by nanowires [8,20,33], these PtCu networks exhibit higher ECSAs due to their smaller nanowire diameter and jagged surface. The ORR measurements were conducted in O_2-satured 0.1 M $HClO_4$ solution at room temperature with a sweep rate of 10 mV s^{-1}. Fig. 4b shows the ORR polarization curves for these PtCu networks, commercial Pt/C, and Pt black catalysts. The half-wave potential of $Pt_{76}Cu_{24}$, $Pt_{52}Cu_{48}$, $Pt_{28}Cu_{72}$, Pt/C, and Pt black catalysts are 0.906, 0.895, 0.886, 0.864, and 0.869 V, respectively. This indicates that all PtCu networks exhibit higher activity than that of the commercial Pt/C and Pt black catalysts, and $Pt_{76}Cu_{24}$ networks display the highest activity among these five catalysts. On the basis of the Levich-Koutecky equation [34,35], the kinetic currents from the ORR polarization curves were calculated and then normalized with respect to the Pt loading mass and ECSA to obtain the mass activity and specific activity, respectively (Table S2). Fig. 4c shows the mass activities of these five catalysts. $Pt_{76}Cu_{24}$ networks exhibit an extraordinary mass activity of 0.466 A mg_{Pt}^{-1}, which is 1.5, 1.8, 4.6, and 11.1 times greater than that of $Pt_{52}Cu_{48}$ networks (0.312 A mg_{Pt}^{-1}), $Pt_{28}Cu_{72}$ networks (0.258 A mg_{Pt}^{-1}), commercial Pt/C (0.102 A mg_{Pt}^{-1}) and Pt black (0.042 A mg_{Pt}^{-1}), respectively. As shown in Fig. 4 d, the specific activities for these various catalysts exhibit similar trends to that of the mass activities. The specific activity of $Pt_{76}Cu_{24}$ (1.273 mA cm^{-2}) is 1.3, 1.4, 7.4, and 5.6 times greater than that of $Pt_{52}Cu_{48}$ networks (0.994 mA cm^{-2}), $Pt_{28}Cu_{72}$ networks (0.878 mA cm^{-2}) commercial Pt/C (0.173 mA cm^{-2}) and Pt black (0.227 mA cm^{-2}), respectively.

Since the electrochemical durability is recognized as one of the most critical issues for the widespread adoption of PEMFCs [2,6,7,36,37], accelerated durability tests (ADTs) were also evaluated by performing 6000 potential cycles between 0.6 and 1.1 V versus a reversible hydrogen electrode (RHE) in O_2-satured 0.1 M $HClO_4$ solution at room temperature with a sweep rate of 50 mV s^{-1}. Fig. 5a-c show the CV curves of the $Pt_{76}Cu_{24}$ networks, commercial Pt/C and Pt black catalysts before and after ADTs. After increased numbers of CV cycles, both commercial Pt/C and Pt black catalysts display dramatic drops for the currents of the peaks in the hydrogen adsorption/desorption potential regions between 0–0.37 V vs RHE (Fig. 5a,b). In contrast, the currents of the peaks in the same potential regions for $Pt_{76}Cu_{24}$ networks exhibit only a slight drop (Fig. 5c). As shown in Fig. 5 d, $Pt_{76}Cu_{24}$ networks display a loss of only 14.9% in their ECSA after 6000 potential cycles,

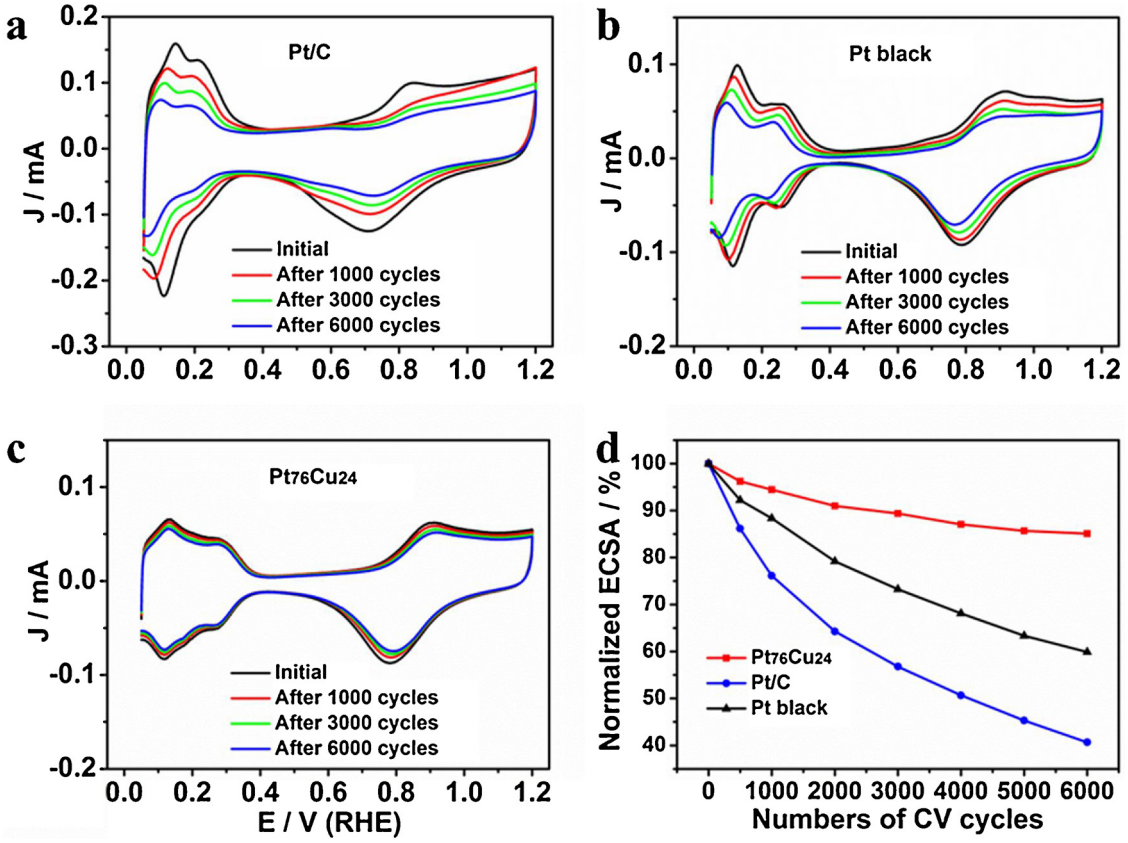

Fig. 5. CV curves for (a) commercial Pt/C catalyst, (b) commercial Pt black catalyst, and (c) $Pt_{76}Cu_{24}$ networks before and after various numbers of cycles. The durability tests were conducted at room temperature in O_2-saturated 0.1 M $HClO_4$ at a scan rate of 50 mV s^{-1} between 0.6 and 1.1 V versus RHE. (d) Loss of ECSA of Pt/C, Pt black, and $Pt_{76}Cu_{24}$ networks after various numbers of CV cycles.

while the ECSAs of commercial Pt/C and Pt black catalysts show significant losses of 59.3% and 40.1%, respectively. Moreover, 70.2% of the initial mass activity is retained for $Pt_{76}Cu_{24}$ networks after ADT (Fig. S8), while 15.1% and 19.0% are observed for commercial Pt/C and Pt black catalysts, respectively. These results definitively reveal that the electrochemical durability of $Pt_{76}Cu_{24}$ networks is also much better than that of the two commercial catalysts of Pt/C and Pt black. To elucidate the reasons for their different durabilities, the morphologies of these catalysts after durability tests were also investigated with TEM. After ADT, the morphology of $Pt_{76}Cu_{24}$ networks shows no obvious change (Fig. S9), whereas serious aggregation/sintering are presented for both commercial Pt/C and Pt black catalysts (Fig. S10), resulting in the significant decreases of their ECSAs. In addition, the surface chemical states of $Pt_{76}Cu_{24}$ networks remain almost the same after ADT (Fig. S11), indicating their high stability. Overall, in comparison with commercial catalysts of Pt/C and Pt black, $Pt_{76}Cu_{24}$ networks have demonstrated a greatly enhanced activity, stability, and durability toward ORR.

Besides bimetallic porous nanowire networks, our strategy can also be facilely extended to prepare trimetallic PtCuAu porous networks with well-defined nanowire structures. The synthesis procedure of PtCuAu nanowire networks was similar to that of $Pt_{76}Cu_{24}$ networks, except that $HAuCl_4$ was supplied together with H_2PtCl_6 and $CuCl_2$. The SEM and TEM images reveal that the products, similarly to bimetallic PtCu, have a typical 3D porous nanostructure with uniform nanowire networks and high dispersity (Fig. 6a,b). The average diameter of the nanowire units is 5.2 nm. The HRTEM image shows that the porous networks exhibit high crystallinity and very jagged nanowire surfaces with plentiful exposed atomic boundaries and corners (Fig. 6c), which can act as highly active catalytic sites. Fig. 6d shows the elemental mapping of an individual nanowire by HAADF-STEM-EDX analyses, which clearly indicates that Pt and Cu elements are distributed wholly while Au elements are concentrated in the center. Moreover, the high crystallinity and trimetallic composition of PtCuAu can be further confirmed by the XRD pattern (Fig. 6e). Notably, PtCuAu networks exhibit much superior ORR activity in comparison with commercial Pt/C and Pt black catalysts (Fig. 6f,g and Fig. S12). Taken together, the simple and efficient strategy described here can be easily extended from bimetals to trimetals, demonstrating its universality for preparation of novel 3D porous nanostructures.

4. Conclusions

In conclusion, we have proposed a convenient and efficient synthesis strategy for 3D highly porous PtCu networks with ultrathin jagged nanowire nanostructures and tunable compositions. The growth mechanism involved in the morphological evolution and roles of the reagents have been fully explored and discussed. The as-synthesized $Pt_{76}Cu_{24}$ networks demonstrate much higher activity, stability and durability in ORR compared to commercial Pt/C and Pt black catalysts. The outstanding ORR performance can be ascribed to the core-shell alloyed structures with a Pt-skin, the 3D networks with high surface area and high porosity, and the ultrathin and jagged nanowires with abundant active atoms. Significantly, trimetallic PtCuAu with well-

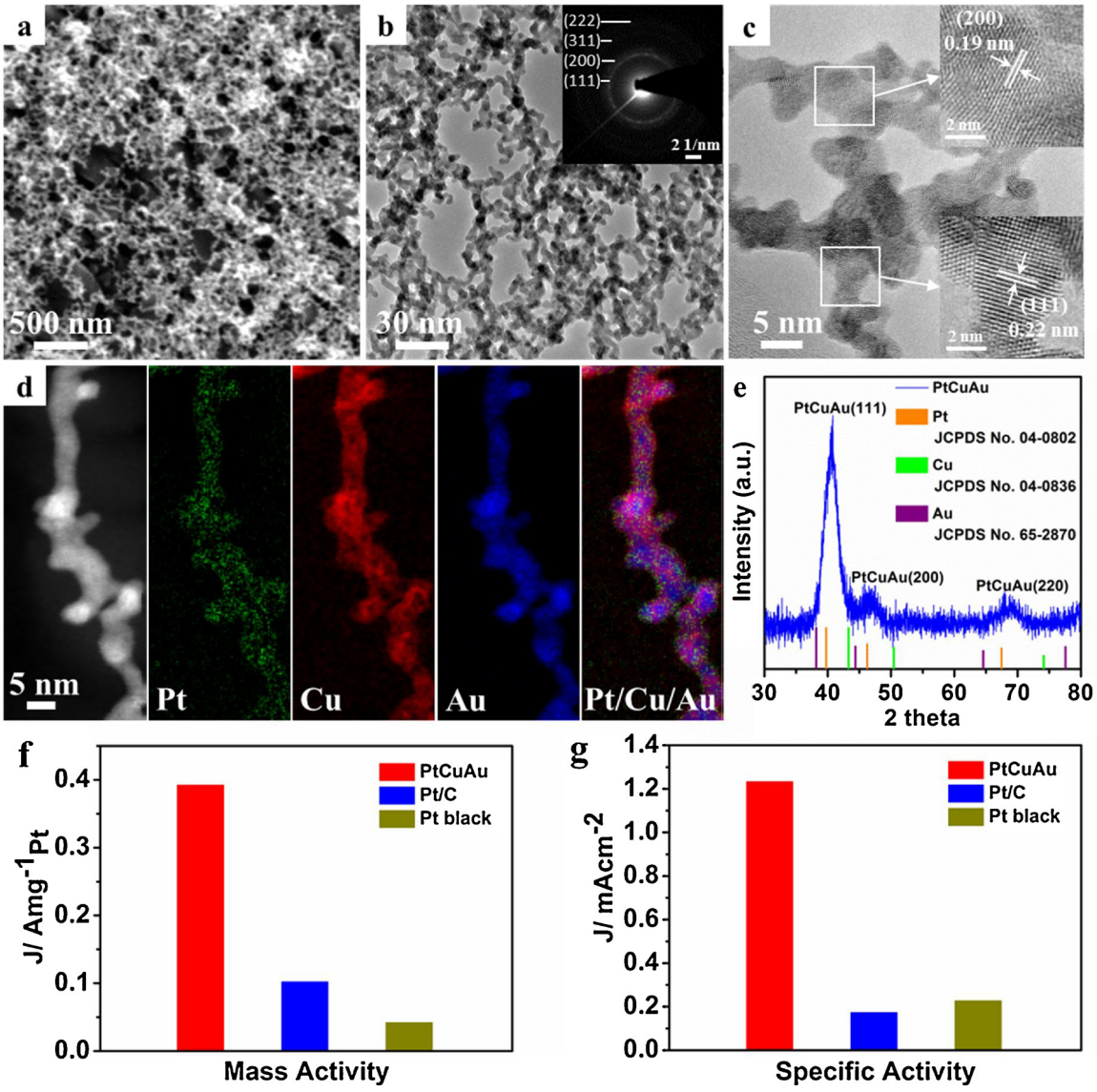

Fig. 6. (a) SEM and (b,c) TEM images of as-synthesized PtCuAu networks. Inset in b) is the SAED pattern recorded from b). (d) HAADF-STEM image and EDX mapping images of an individual nanowire in as-synthesized PtCuAu networks. (e) XRD pattern of PtCuAu networks. (f) Mass activity and (g) specific activity at 0.9 V versus RHE for PtCuAu, Pt/C, and Pt black catalysts.

defined 3D porous networks could also be easily prepared using this synthesis strategy, which demonstrates its flexibility for novel 3D porous nanoarchitectures with great potential in various catalytic applications.

Acknowledgments

This work was supported by the Natural Sciences and Engineering Research Council of Canada (NSERC), the University of Waterloo, and the Waterloo Institute for Nanotechnology. The authors greatly acknowledge the Catalysis Research for Polymer Electrolyte Fuel Cells (CaRPE FC) Network administered from Simon Fraser Grant No. APCPJ 417858-11 through NSERC.

Appendix A. Supplementary data

Supplementary material related to this article can be found, in the online version, at doi:https://doi.org/10.1016/j.apcatb.2018.04.035.

References

[1] A. Chen, P. Holt-Hindle, Platinum-based nanostructured materials: synthesis, properties, and applications, Chem. Rev. 110 (2010) 3767–3804.
[2] Y. Nie, L. Li, Z. Wei, Recent advancements in Pt and Pt-free catalysts for oxygen reduction reaction, Chem. Soc. Rev. 44 (2015) 2168–2201.
[3] W. Yu, M.D. Porosoff, J.G. Chen, Review of Pt-based bimetallic catalysis: from model surfaces to supported catalysts, Chem. Rev. 112 (2012) 5780–5817.
[4] J. Ying, G. Jiang, Z.P. Cano, L. Han, X.-Y. Yang, Z. Chen, Nitrogen-doped hollow porous carbon polyhedrons embedded with highly dispersed Pt nanoparticles as a highly efficient and stable hydrogen evolution electrocatalyst, Nano Energy 40 (2017) 88–94.
[5] J. Ying, J. Li, G. Jiang, Z.P. Cano, Z. Ma, C. Zhong, D. Su, Z. Chen, Metal-organic frameworks derived platinum-cobalt bimetallic nanoparticles in nitrogen-doped hollow porous carbon capsules as a highly active and durable catalyst for oxygen reduction reaction, Appl. Catal. B-Environ. 225 (2018) 496–503.
[6] M.K. Debe, Electrocatalyst approaches and challenges for automotive fuel cells, Nature 486 (2012) 43–51.
[7] M. Shao, Q. Chang, J.-P. Dodelet, R. Chenitz, Recent advances in electrocatalysts for oxygen reduction reaction, Chem. Rev. 116 (2016) 3594–3657.
[8] H.W. Liang, X. Cao, F. Zhou, C.H. Cui, W.J. Zhang, S.H. Yu, A free-standing Pt-nanowire membrane as a highly stable electrocatalyst for the oxygen reduction reaction, Adv. Mater. 23 (2011) 1467–1471.
[9] L. Wang, Y. Nemoto, Y. Yamauchi, Direct synthesis of spatially-controlled Pt-on-Pd bimetallic nanodendrites with superior electrocatalytic activity, J. Am. Chem. Soc. 133 (2011) 9674–9677.

[10] X. Huang, E. Zhu, Y. Chen, Y. Li, C.Y. Chiu, Y. Xu, Z. Lin, X. Duan, Y. Huang, A facile strategy to Pt_3Ni nanocrystals with highly porous features as an enhanced oxygen reduction reaction catalyst, Adv. Mater. 25 (2013) 2974–2979.
[11] Z. Chen, M. Waje, W. Li, Y. Yan, Supportless Pt and PtPd nanotubes as electrocatalysts for oxygen reduction reactions, Angew. Chem. Int. Ed. 46 (2007) 4060–4063.
[12] S.M. Alia, G. Zhang, D. Kisailus, D. Li, S. Gu, K. Jensen, Y. Yan, Porous platinum nanotubes for oxygen reduction and methanol oxidation reactions, Adv. Funct. Mater. 20 (2010) 3742–3746.
[13] C. Chen, Y. Kang, Z. Huo, Z. Zhu, W. Huang, H.L. Xin, J.D. Snyder, D. Li, J.A. Herron, M. Mavrikakis, Highly crystalline multimetallic nanoframes with three-dimensional electrocatalytic surfaces, Science 343 (2014) 1339–1343.
[14] Z. Niu, N. Becknell, Y. Yu, D. Kim, C. Chen, N. Kornienko, G.A. Somorjai, P. Yang, Anisotropic phase segregation and migration of Pt in nanocrystals en route to nanoframe catalysts, Nat. Mater. 15 (2016) 1188–1194.
[15] H. Wu, H. Li, Y. Zhai, X. Xu, Y. Jin, Facile synthesis of free-standing Pd-based nanomembranes with enhanced catalytic performance for methanol/ethanol oxidation, Adv. Mater. 24 (2012) 1594–1597.
[16] W. Liu, A.K. Herrmann, D. Geiger, L. Borchardt, F. Simon, S. Kaskel, N. Gaponik, A. Eychmüller, High-performance electrocatalysis on palladium aerogels, Angew. Chem. Int. Ed. 51 (2012) 5743–5747.
[17] C. Zhu, Q. Shi, S. Fu, J. Song, H. Xia, D. Du, Y. Lin, Efficient synthesis of MCu (M = Pd, Pt, and Au) aerogels with accelerated gelation kinetics and their high electrocatalytic activity, Adv. Mater. 28 (2016) 8779–8783.
[18] W. Liu, P. Rodriguez, L. Borchardt, A. Foelske, J. Yuan, A.K. Herrmann, D. Geiger, Z. Zheng, S. Kaskel, N. Gaponik, Bimetallic aerogels: high-performance electrocatalysts for the oxygen reduction reaction, Angew. Chem. Int. Ed. 52 (2013) 9849–9852.
[19] M. Li, Z. Zhao, T. Cheng, A. Fortunelli, C.-Y. Chen, R. Yu, Q. Zhang, L. Gu, B.V. Merinov, Z. Lin, Ultrafine jagged platinum nanowires enable ultrahigh mass activity for the oxygen reduction reaction, Science 354 (2016) 1414–1419.
[20] M.A. Hoque, F.M. Hassan, D. Higgins, J.Y. Choi, M. Pritzker, S. Knights, S. Ye, Z. Chen, Multigrain platinum nanowires consisting of oriented nanoparticles anchored on sulfur-doped graphene as a highly active and durable oxygen reduction electrocatalyst, Adv. Mater. 27 (2015) 1229–1234.
[21] Z. Nie, A. Petukhova, E. Kumacheva, Properties and emerging applications of self-assembled structures made from inorganic nanoparticles, Nat. Nanotech. 5 (2010) 15–25.
[22] J. Zhang, C.M. Li, Nanoporous metals: fabrication strategies and advanced electrochemical applications in catalysis, sensing and energy systems, Chem. Soc. Rev. 41 (2012) 7016–7031.
[23] Y. Ding, M. Chen, Nanoporous metals for catalytic and optical applications, MRS Bull. 34 (2009) 569–576.
[24] K.G. Ranmohotti, X. Gao, I.U. Arachchige, Salt-mediated self-assembly of metal nanoshells into monolithic aerogel frameworks, Chem. Mater. 25 (2013) 3528–3534.
[25] D. Wen, W. Liu, D. Haubold, C. Zhu, M. Oschatz, M. Holzschuh, A. Wolf, F. Simon, S. Kaskel, A. Eychmüller, Gold aerogels: three-dimensional assembly of nanoparticles and their use as electrocatalytic interfaces, ACS Nano 10 (2016) 2559–2567.
[26] X. Gao, R.J. Esteves, T.T.H. Luong, R. Jaini, I.U. Arachchige, Oxidation-induced self-assembly of Ag nanoshells into transparent and opaque Ag hydrogels and aerogels, J. Am. Chem. Soc. 136 (2014) 7993–8002.
[27] B.Y. Xia, H.B. Wu, X. Wang, X.W. Lou, One-pot synthesis of cubic $PtCu_3$ nanocages with enhanced electrocatalytic activity for the methanol oxidation reaction, J. Am. Chem. Soc. 134 (2012) 13934–13937.
[28] S.-H. Ye, X.-J. He, L.-X. Ding, Z.-W. Pan, Y.-X. Tong, M. Wu, G.-R. Li, Cu_2O template synthesis of high-performance PtCu alloy yolk–shell cube catalysts for direct methanol fuel cells, Chem. Commun. 50 (2014) 12337–12340.
[29] L. Wang, Y. Yamauchi, Metallic nanocages: synthesis of bimetallic Pt–Pd hollow nanoparticles with dendritic shells by selective chemical etching, J. Am. Chem. Soc. 135 (2013) 16762–16765.
[30] X. Huang, Y. Li, Y. Chen, E. Zhou, Y. Xu, H. Zhou, X. Duan, Y. Huang, Palladium-based nanostructures with highly porous features and perpendicular pore channels as enhanced organic catalysts, Angew. Chem. Int. Ed. 125 (2013) 2580–2584.
[31] J. Ying, X.-Y. Yang, G. Tian, C. Janiak, B.-L. Su, Self-assembly: an option to nanoporous metal nanocrystals, Nanoscale 6 (2014) 13370–13382.
[32] N. Jung, Y. Sohn, J.H. Park, K.S. Nahm, P. Kim, S.J. Yoo, High-performance $PtCu_x$@Pt core-shell nanoparticles decorated with nanoporous Pt surfaces for oxygen reduction reaction, Appl. Catal. B-Environ. 196 (2016) 199–206.
[33] S. Sun, G. Zhang, D. Geng, Y. Chen, M.N. Banis, R. Li, M. Cai, X. Sun, Direct growth of single-crystal Pt nanowires on Sn@CNT nanocable: 3D electrodes for highly active electrocatalysts, Chem. Eur. J. 16 (2010) 829–835.
[34] B. Lim, M. Jiang, P.H. Camargo, E.C. Cho, J. Tao, X. Lu, Y. Zhu, Y. Xia, Pd-Pt bimetallic nanodendrites with high activity for oxygen reduction, Science 324 (2009) 1302–1305.
[35] J. Ying, X.-Y. Yang, Z.-Y. Hu, S.-C. Mu, C. Janiak, W. Geng, M. Pan, X. Ke, G. Van Tendeloo, B.-L. Su, One particle@one cell: highly monodispersed PtPd bimetallic nanoparticles for enhanced oxygen reduction reaction, Nano Energy 8 (2014) 214–222.
[36] K.A. Kuttiyiel, K. Sasaki, G.-G. Park, M.B. Vukmirovic, L. Wu, Y. Zhu, J.G. Chen, R.R. Adzic, Janus structured Pt–FeNC nanoparticles as a catalyst for the oxygen reduction reaction, Chem. Commun. 53 (2017) 1660–1663.
[37] J. Ying, Z.-Y. Hu, X.-Y. Yang, H. Wei, Y.-X. Xiao, C. Janiak, S.-C. Mu, G. Tian, M. Pan, G. Van Tendeloo, High viscosity to highly dispersed PtPd bimetallic nanocrystals for enhanced catalytic activity and stability, Chem. Commun. 52 (2016) 8219–8222.